Shinsaku Tada

Texte, Inc, Tokyo, Japan

E-mail: s-tada@texte.co.jp

Water transport in air-pores

ABSTRACT: Water transport experiments were performed on AAC with known pore structure and well-controlled moisture content. Specimens with the critical moisture content for freeze/thaw resistance were observed with the cryo-SEM. Evidences were confirmed that the ice segregated on the surface of air-pores as a result of redistribution of unfrozen water coming from the matrix part between air-pores. The standpipe absorptivity test for specimens with an air-pore volume of approx. 45 vol.% while having different mean air-pores diameters showed an abrupt jump of permeability when the mean air-pores diameter was smaller than 0.15 mm or the air-pores connectivity was 20%. In the free water uptake test using a dried AAC specimen, the capillary suction precedes other water transports and saturates the capillaries of 35 vol. % instantly followed by a slow absorption process, i.e. escaping of entrapped air bubbles that controls the subsequent absorption rate.

KEY WORDS: autoclaved aerated concrete, Cryo-SEM, Ice formation, air pore, entrapped air, sorptivity, standpipe absorptivity

1. Introduction

Air-pore structure of AAC has been well documented in terms of compressive strength [1] and thermal performance [2] while little is known regarding water transport behaviour, probably because air-pores are large enough not to be acting as a capillary [3]. This study emphasizes the role of air-pores in water transport based on the three experiments: water redistribution around unsaturated air-pores during freezing, threshold air-pores connectivity for water penetration and entrapped air dissolution during absorption. Low-temperature SEM observation of unsaturated AAC during freezing with a moisture content of 35 vol.% showed considerable ice segregation in air-pores implying unfrozen capillary water redistribution and stress relaxation. It was also shown that mean air-pores diameter of 0.2 mm with a total air-pores volume of 45 vol.% exhibited abrupt water penetration implying a bond percolation in the connectivity of air-pores. The slow water uptake observed in the latter stage of water absorption test was attributed to the dissolution of the entrapped air bubbles in the water of air-pores.

2. Unfrozen water transport and ice segregation in air-pores

2.1. Observation of air-pore surface during freezing

When unsaturated AAC is subjected to freezing, water held in large pores enough to freeze without freezing point depression freezes first and subsequent freezing extends gradually over smaller pores [4]. The unfrozen adsorbed or capillary water that exhibits freezing point depression due to surface forces of the solid shows a tendency to migrate towards ice as the chemical potential of ice decreases with a decrease of temperature, leading to a redistribution of water inside of a specimen without external water supply. The air-pores will provide unfrozen water with spaces for ice segregation.

A schematic image of AAC with a different degree of saturation S under freezing temperatures is shown in Fig. 1. It is shown (Fig. 1(b)) that moisture in a specimen saturates capillary pores but not extends over air-pores except for very fine size pores. When specimen temperature decreases lower than the freezing temperature of free water, the capillary water begins to freeze and segregates in the air-pores. The direct observation of ice segregated in an air-pore was shown by Gruble [5] but the moisture content of the specimen during freezing was not specified and the conditions to obtain the observed surface was not reported. Corr et al [6] and Monteiro et al. [7] conducted series of experiments with a cryo-SEM but the moisture condition was not controlled. In this study, the moisture content of specimen was controlled to be close to that shown in Fig. 1(b). The specimen was then subjected to freezing and observed with a cryo-SEM.

AAC specimens with a bulk density of 486 kg/m^3 and 638 kg/m^3 were prepared using pre-foaming method in the laboratory while those of gas-foaming type with a bulk density of 492 kg/m^3 were a commercial product. The production conditions of the specimen are shown in Table 1. In this experiment, specimen with a bulk density of 486 kg/m^3 was used and cut out in a 7mm in length and 5 mm in diameter. They were first vacuum-saturated in water followed by a gradual drying to have a degree of saturation of 47.5%. The specimens were sealed and left in a freezing chamber at -15°C for three days and then introduced to the specimen chamber of the field emission scanning electron microscope (Hitachi S-800) with a cryo-stage that was able to cool specimens to the liquid nitrogen temperature. Vacuumed at a pressure of 0.8 torr, the specimen was cut in the specimen chamber to have a fresh cross-section for observation. The acceleration voltage was 5kV and no gold deposition was applied.

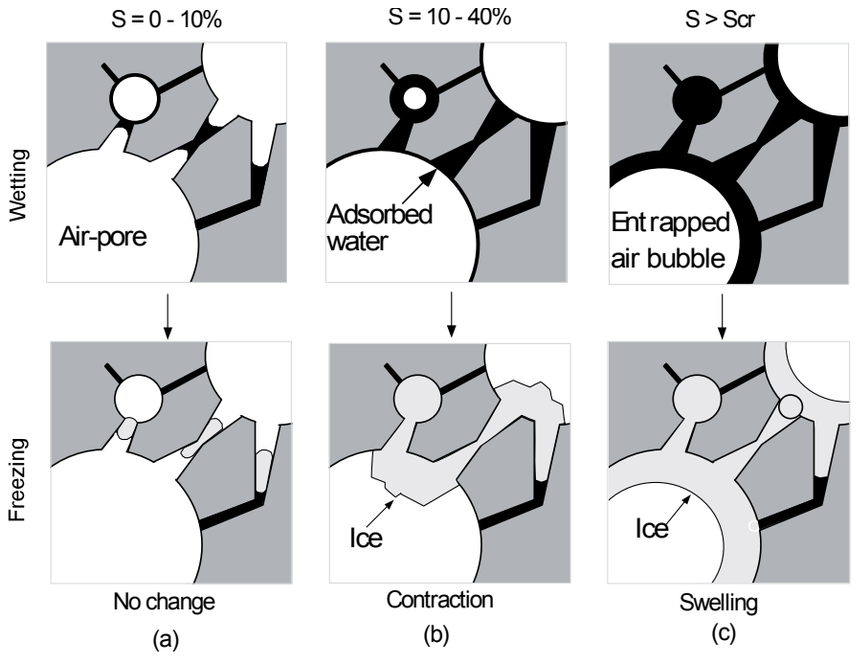

Fig. 1. Water distribution in air-pores before and after freezing.

Normally frost damage to AAC occurs after several freeze/thaw cycles. However, major contribution of the freeze/thaw cycles is to increase moisture content to a critical degree of saturation S_{cr} [8] where only one freezing could cause frost damage. Hence just one freezing, employed in this experiment, is a sufficient condition to observe ice formation at the instant of frost damage.

2.2. Results of the cryo-sem observation of ice formation

The degree of saturation of the specimen was 47.5 (38 vol.%) which was controlled to be close to the critical degree of saturation for freeze-thaw resistance as defined by RILEM recommendation. At this moisture condition, the capillary pores of 35 vol.% located in the matrix part between air-pores are fully saturated and some small air-pores may also be saturated [9]. The surface of air-pores frozen at this moisture condition is shown in Fig. 2(a) and (b). At the center of Fig. 2(a), a large air-pore shows small amount of ice while the other smaller air-pores on the right show considerable ice formation. Figure 2(b) is a two-time magnified view of the upper-right part of Fig. 2(a).

The preliminary optical microscope observation showed that no water existed in such air-pores before freezing, hence the observed ice is supposed to come from the matrix part behind the air-pores. On the surface of the largest air-pore in Fig. 2(a), several parts show no ice formation, which is highlighted with a white dashed circle. It is obvious that this part has a hole behind which may be generated as a result of overlapping of air-pores. This channel plays an important role in the downward water absorption test as discussed later.

The ice observed on the surface of air-pores may come from the capillary pores between air-pores hence no ice can be formed in the channel that has no capillary pores behind. A straightforward evidence of the unfrozen water migration is shown in Fig. 2(b) as highlighted with a white circle, where the cross-section of the channel is clearly shown without any ice segregations.

2.3. Discussion

Specimen with a moisture content of the critical degree of saturation for freeze/thaw resistance still contains ice-filled air-pores with a diameter less than 150 μm as shown in Fig. 2(b) forming a hollow sphere of thick ice shell. Moreover the small air-pore shown in the right side of Fig. 2(a) is fully occupied with ice where unfrozen water migration from the matrix part is no longer possible resulting in a partial increase in hydraulic pressure. This corresponds with the fact that the specimen with a moisture content of S_{cr} showed expansion first among others with a lower moisture content exhibiting contraction [10].

As well known, unfrozen water in an unsaturated porous material shows redistribution during freezing and freezes into ice at large pores such as air bubbles. This is a major reason of the availability of entrained air for frost resistance of concrete. However, when its moisture content exceeds a certain limit, the air bubbles can no longer mitigate the hydraulic pressure, as directly shown in this experiment.

3. Standpipe absorptivity and air-pore structure

3.1. Introduction

AAC specimens with various air-pore structure and a fixed bulk density of approx. 500 kg/m^3 (total porosity of approx. 80%) were prepared using seven types of foaming agent A to G. The dimension of the specimens were 160 x 160 x 40 mm. Because the bulk density was fixed, air-pores volumes of the specimens were the same. However, due to the difference in the type of foaming agent,

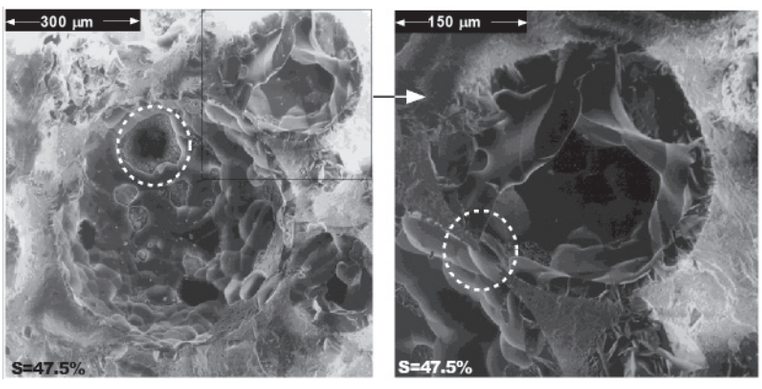

Fig. 2. Ice segregation in air-pores of unsaturated AAC.

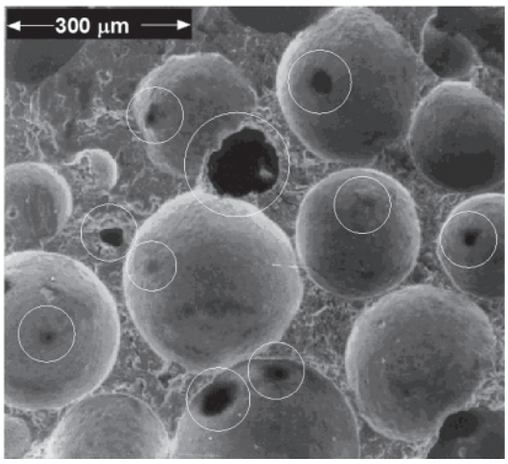

Fig. 3. Macoscopic channels between air-pores observed with SEM.

air-pores size distributions were different, which was supposed to have some impact on the standpipe absorptivity.

3.2. Test condition

The standpipe absorptivity test was performed with a water-filled graduated cylinder standing on a specimen with a dimension of was 160 x 160 x 40 mm and the decease in the water level was recorded with time. A supplementary immersion test was also performed using specimens with a dimension of 100 x 100 x 100 mm, which was immersed in water 100 mm below the water level and the increase in the water content was recorded with time. Another specimens were cut out to have a cross-section for image analysis with an observation area of 8 x 6 mm. A sufficient contrast of air-pores was obtained simply by emitting visible light from the lateral direction. The video images were subjected to image analysis and the area fractions of air-pores and the apparent mean diameters were calculated. The area fraction of air-pore corresponds to that of volume fraction according to the stereology principle while apparent mean air-pores diameters (0.142 mm to 0.285 mm) were not reliable because the cross-sections did not always show true diameter. Hence the connectivity between air-pores cannot be discussed in terms of the apparent mean air-pores diameters. Instead a new concept of air-pores connectivity was introduced. As shown in Fig. 3, number of holes originated from the overlapping of air-pores, white circles on the scanning electron micrograph, were counted per unit area and named as the air-pores connectivity index.

3.3. Results of the standpipe absorptivity test

Results are shown in Table 1 and the relationship between standpipe absorptivity and air-pore connectivity index is shown in Fig. 4. It is clearly shown that the standpipe absorptivity shows considerable increase when the air-pores connectivity index exceeds 20% implying the establishment of the first overall interconnection of air-pores. A similar tendency is also found in the relationship between the apparent mean air-pores diameter and the standpipe absorptivity as shown in Fig. 5 where the abrupt increase in the standpipe absorptivity is shown at an apparent mean air-pores diameter of 0.15 mm. This is a transition phenomenon where a volume-filling parameter such as air-pores size distribution causes abrupt property jump and may be an experimental evidence of a percolation threshold.

3.4. Discussion

In the standpipe absorptivity test, a pressure head is applied to the upper surface of a specimen and any defects such as air-pore connection channels, if any, drive water more quickly and massively than capillary suction. Hence the test can evaluate the macroscopic pore continuity such as air-pores connectivity. However, in the water immersion test, the capillary suction and the macroscopic channel drive water simultaneously hence the experimental results provide less information on the relationship between pore structure and water transport characteristics. In the free water uptake test as described later, capillary suction dominates the entire flows rather than gravity-driven flow and the effect of air-pore structure would be manifested as the dissolution of entrapped air that are left behind by the capillary flows. It is shown in this experiment that an abrupt decrease in resistance to the gravity-driven flow may occur associated with an increase in air-pores connectivity when the apparent mean air-pores diameter lowers a limit value.

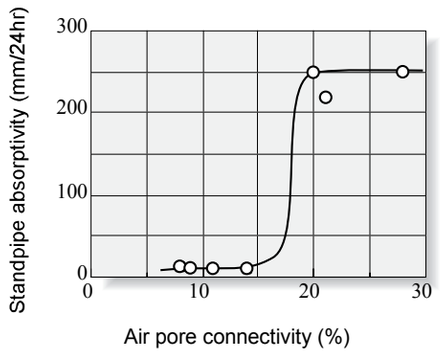

Fig. 4. Relationship between standpipe absorptivity and air-pores connectivity.

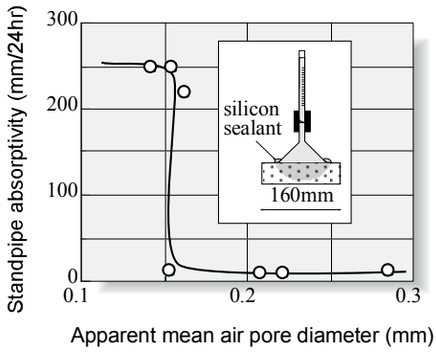

Fig. 5. Relationship between standpipe absorptivity and apparent mean air-pores diameter.

Table 1

AAC SPECIMEN.

Foaming method	Bulk density (kg/m^3)	Total porosity	Raw materials	Curing method
Gas foaming	492	0.810	Quartz powder, Portland cement, Aluminium powder	Autoclave curing 180°C, 10 atm, 8 hours
Pre-foaming	486	0.815	Quartz powder, Portland cement, Quick setting agent, Surfactant agent	
Pre-foaming	638	0.757		

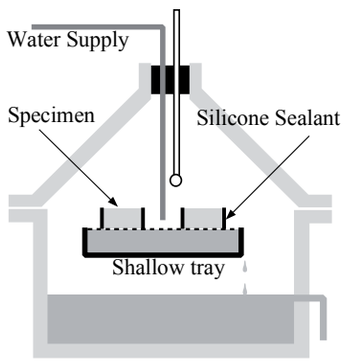

Fig. 6. Apparatus for the free water uptake test.

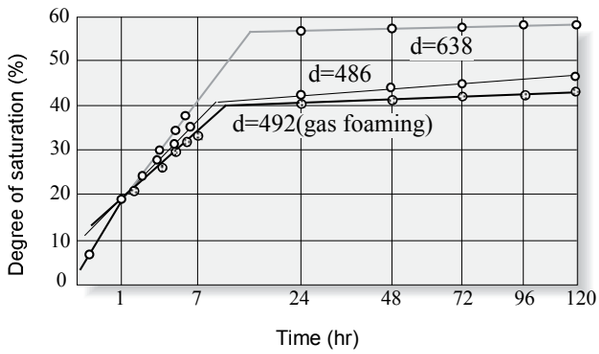

Fig. 7. Water absorption rate of various types of AAC.

4. Capillary water uptake and entrapped air bubbles

4.1. Free water uptake test

When water is sucked form the bottom of an AAC specimen solely by capillary suction, the well-known two straight lines of the relationship between moisture content and square root of time can be observed. The first straight line has been attributed to the sorptivity [11] while the meaning of the other straight line observed at the latter stage of absorption still needs discussions. In this study, AAC specimens with different capillary and air-pores volumes were prepared and examine the later-stage absorption behavior with the free water uptake tests.

4.2. Test conditions

Three types of AAC specimens with different bulk densities and foaming methods were prepared as shown in Table 1. The dimension of the specimen was 100 mm in diameter and 40 mm in thickness cut out from a cylinder of 100 mm in diameter and 200 mm in height and the surface was sealed with a silicone type sealant except for the upper and bottom side to keep cutout surfaces. Specimens were placed in a glass desiccator to avoid drying and the shallow tray with a stainless steel mesh supporting the specimens makes it possible to keep water level constant as shown in Fig. 6. Because the top surface is the original cutout surface, permeability of gas is not interfered and the glass desiccator allows observation of the top surface of the specimen during water absorption. The specimens were taken out at specified intervals, the bottom surface was wiped softly with a PVA foam and then the specimens were weighed quickly.

4.3. Result of the free water uptake test

The test result is shown in Fig. 7 where absorption rate depends on both bulk density d and pore structure. In the case of specimen with a bulk density of d=486 kg/m^3, entire capillary pore of 35 vl.% was filled quickly at the first 10 hours by the capillary suction. Because the moisture condition in this figure is expressed in terms of saturation, volume of water by the total pore volume, the measured values in the figure can be converted to volumetric moisture content by multiplying the total porosity. The broken two straight lines both show changes in moisture content with square-root of time and suggest two different diffusion mechanisms.

The abrupt absorption rate observed immediately after the specimen-water contact is well known as the sorptivity. At the end of

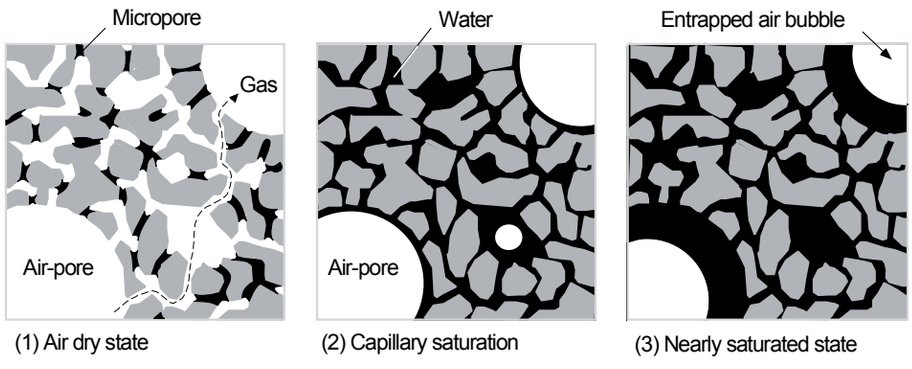

Fig. 8. Schematic view of pore structure, water and air in unsaturated AAC.

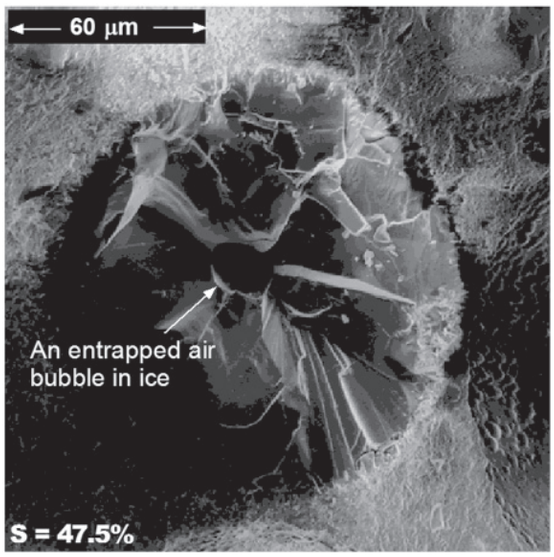

Fig. 9. Direct observation of an entrapped air bubble in ice (see Fig. 8(2))..

this process, i.e. 10 hours later in this experiment, water reached the top surface and the specimen exhibited a wet color while the moisture content was not as high as 80 vol.% that is the total pore volume of the specimen. Hence it is concluded that considerable air still remain in the specimen

4.4. Discussions

A stage of moderate increase in water content observed after the rapid absorption has been attributed to the diffusion of water to a finer gel pores [12] or to the escape of air through macroscopic channels [13]. It is, however, more realistic to take it a gradual dissolution of entrapped air and associated volume change can be compensated with incoming water [9, 15].

Configurations of water and air at different degree of saturations are schematically shown in Fig. 8. When water is in contact with a dried specimen, it migrates quickly through the capillary pores distributed in the matrix between air-pores, and the air inside of the air-pores is likely to be left as bubbles in water. The cryo-SEM observation of a cutout surface of an unsaturated frozen AAC also demonstrated a bubble-like spherical cross section within ice in an air-pore as shown in Fig. 9. This ice-air configuration agrees well with the predicted one shown in Fig. 8(2).

Diameter of the entrapped air bubbles tends to be larger when the host air-pores are large. The dissolution rate of air in the entrapped air bubble becomes slow when the diameter of air bubble becomes larger resulting in slower water uptake. For comparison, AAC specimens with different mean air-pores diameters were tested in this experiment while their bulk densities are very close, 486 and 492 kg/m^3, showing the total air-pores volume is the same. At the first stage of quick absorption, the sorptivity is almost the same while at the second stage, the water absorption slope is gentler in specimen with a larger mean air-pores diameter where air dissolution rate is slow as shown in Fig. 7.

5. Conclusions

The total porosity of AAC with a bulk density of approx. 500 kg/m^3 extends over 80%. The pores volume comprises air-pores of 45% and capillary pores of 35%. This study was designed to execute various water transport experiments under well-defined pore structure and well-controlled moisture content.

A reverse from contraction to expansion may occur in unsaturated porous hydrophilic bodies at a critical moisture content. AAC specimens were prepared to have the critical moisture content and observed with the cryo-SEM. Some evidences were confirmed that the ice segregated on the surface of air-pores could be a result of redistribution of unfrozen capillary water coming from the matrix part between air-pores.

When water is applied downward, the gravity-driven bulk flow may exceed the capillary flow provided that a sufficient amount of macroscopic channels develop between air-pores leading to an early-stage saturation. The standpipe absorptivity test was performed for AAC specimens with an air-pores volume of approx. 45 vol.% while having different mean air-pores diameters. The permeability exhibited an abrupt jump when the mean air-pores diameter was smaller than 0.15 mm that corresponded to the air-pores connectivity of 20%. The critical air-pores connectivity that provides a number of air-pores channels from the top to the bottom of the specimen could cause such a transition phenomenon.

In the free water uptake test using a dried AAC specimen, the capillary suction precedes other water transports and saturates the capillary pore of 35 vol.% instantly, followed by a slow absorption process, i.e. escaping or dissolution of air entrapped in air-pores, that controls the subsequent absorption rate until the full saturation.

Bibliography

[1] Kunhanandan Nambiar, E. K. and Ramamurthy, K. 2007. Air-void characterisation of foam concrete. Cement and Concrete Research. **37**, 221-230.

[2] Laurent, J. - P., 1991. La conductivité thermique ‘a sec’ des bétons cellulaires autoclavés: Un modéle conceptual. Materials and Structures. **24**, 221-226.

[3] Kunhanandan Nambiar, E. K. and Ramamurthy, K., 2007. Sorption characteristics of foam concrete. Cement and Concrete Research. **37**, 1341-1347.

[4] Picket, G., 1953. Flow of moisture in hardened portland cement during freezing. Proc. Highway Research Board. **32**, 276-284.

[5] Gruble, P., 1981. Uber die Rolle des Eises in Gefuge Zemengebundener Baustoffe. Beton. **31 (2)**, 54-58.

[6] Corr, D. J., Monteiro, P. J. M. and Bastacky, J., 2002. Microscopic characterization of ice morphology in entrained air voids. ACI Materials Journal. **99 (2)**, 190-195.

[7] Monteiro, P. J. M., Coussy, O. and Silva, D. A., 2006. Effect of cryo-suction and air void transition layer on hydraulic pressure of freezing concrete. ACI Materials Journal. **103 (2)**, 136-140.

[8] Fagerlund, G., 1978. The critical degree of saturation method assessing the freez/thaw resistance of concrete. Materials and Structures. **10 (58)**, 217-229.

[9] Tada, S. and Nakano, S., 1983. Microstructural approach to properties of moist cellular concrete. Autoclaved Aerated Concrete -Moisture and Properties. ed. F. H. Wittmann, Elsevier. 71-88.

[10] Tada, S., 1996. Microstructural approach to frost resistance of highly porous materials. Proc. 7th Int. Conf. Durability Build. Mater. Components. Stockholm. **Vol. 1**, 299-308.

[11] Hall, C. 1989. Water sorptivity of mortar and concrete: A review. Magazine of Concrete Research. **41** (147), 51-61.

[12] Martys, N. S. and Ferraris, C. F., 1997. Capillary transport in mortars and concrete. Cement and Concrete Research. **27 (5)**, 747-760.

[13] Hall, C. and Hoff, W., 2002. Water transport in brick, stone and concrete. Spon Press, London and New York.

[14] Bomberg, M., 1974. Moisture flow through porous building materials. Lund Institute of Technology. Report 52.